Modeling of Non-Isothermal Film Blowing Process for Polyolefines by Using Variational Principles

Roman Kolarik and Martin Zatloukal

Polymer Centre, Faculty of Technology, Tomas Bata University in Zlín, TGM 275, 762 72 Zlín, Czech Republic

Abstract. In this work, film blowing process analysis has been performed theoretically by using minimum energy approach for non-Newtonian polymer melts considering non-isothermal processing conditions and the obtained predictions were compared with both, theoretical and experimental data (bubble shape, velocity and temperature profiles) taken from the open literature. It has been found that model predictions are in very good agreement with the corresponding experimental data.

Keywords: Non-isothermal film blowing, Polymer processing modeling, Variational principles.
PACS: 47.50.-d, 83.10.Gr, 83.50.Uv, 83.60.St, 83.80.Sg

INTRODUCTION

The film blowing process is widely applied for a production of biaxially-oriented thin polymeric films. The film manufacture starts in extruder, where polymer pellets are transported from a hopper to an annular die by a screw. Subsequently, the polymer melt is formed to a continuous tube. At this moment, bubble is still in a molten state and it is oriented in two directions: in the machine direction by the nip rolls and in the circumferential direction by an internal air pressure. Simultaneously, bubble is cooled by a cooling ring situated around the bubble. This happens until a freeze line height is not achieved. Then, the film is in a solid state. The dimensions of the bubble are defined by the terms *blow-up ratio*, which is the ratio of the final bubble diameter at the freeze line height to the bubble diameter at the die exit, and the *take-up ratio*, which is the ratio of the film velocity above the freeze line to melt velocity through die exit. Further, the bubble is compound between two table flaps. Then, film is drawn to a wind-up device by nip and guide rolls. A description of the process is shown schematically in Figure 1. The final film created in this way, can be applied in a food processing, as well as, in a health service or waste industry. Although, the film blowing process has been continuously developing from latest 1930´s, even now the process is not fully understood yet because there are some problems, which bring significant processing limitations [1-12], such as bubble instabilities [1-27]. The most popular way to optimize the film blowing process is modeling. Many film blowing models are based on Pearson and Petrie formulation [18-20] which considers the film

CP1152, *Novel Trends in Rheology III – Proceedings of the International Conference,* edited by M. Zatloukal

as a thin shell in tension from internal air pressure and film drawing. Unfortunately, this formulation has limited capability in describing the full range of bubble shapes observed experimentally and may lead to variety of numerical instabilities. Thus, the Zatloukal-Vlcek model [28-31] has been developed and used to overcome these difficulties by the help of variational principles, where the stable bubble has to satisfy minimum energy requirements. The main idea of this paper is to test non-isothermal Zatloukal-Vlcek model considering non-Newtonian polymer melt by using experimental and theoretical data taken from the open literature.

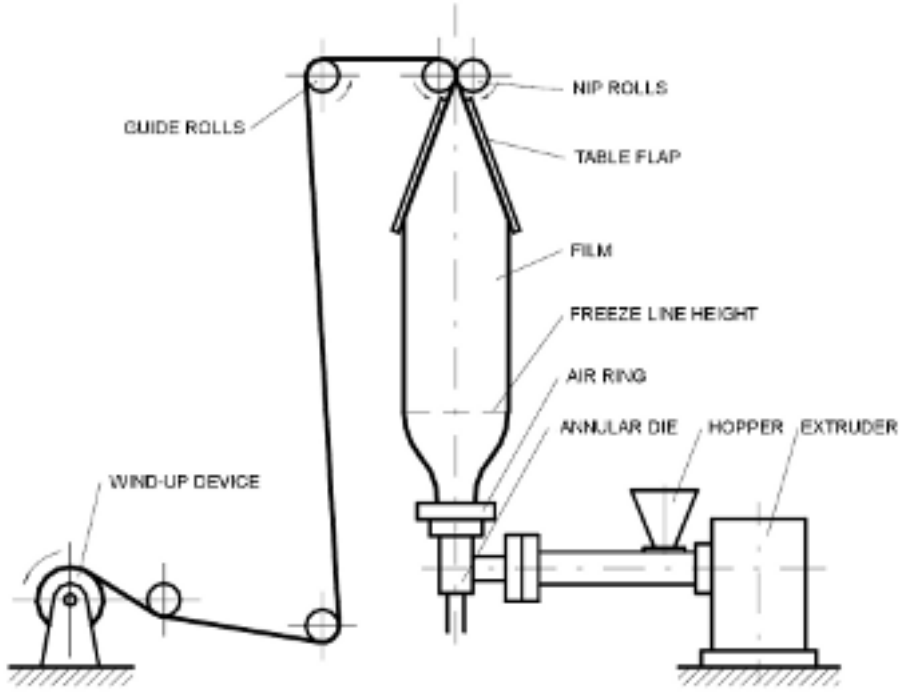

FIGURE 1. The film blowing line.

MATHEMATICAL MODELING

Pearson and Petrie Formulation

The first and probably the most important contribution to modeling of the film blowing process were given by Pearson and Petrie [16, 32] who developed basic and simple kinematic frame of the film blowing process. In their pioneering work, they have employed Newtonian model as the constitutive equation and the process has been assumed to be isothermal. Pearson and Petrie formulation [16] is based on the following assumptions (see Figure 2 for more details):

- Membrane theory: the bubble is described as a thin shell where the film thickness, h, is much smaller than the bubble radius, r ($h << r$).
- The bubble movement is time steady and symmetrical around the bubble axis.
- The surface and inertial stresses are neglected due to their low values.

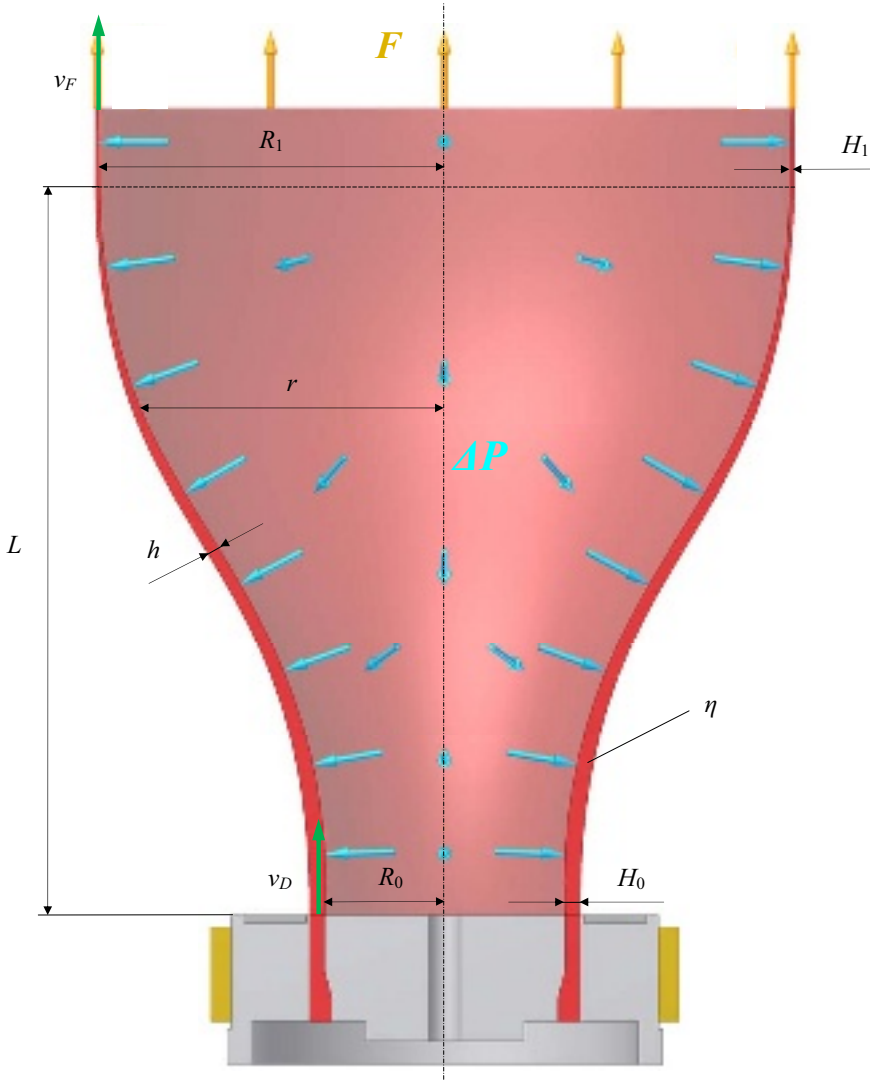

FIGURE 2. Film blowing variables.

The Pearson and Petrie have used a local Cartesian coordinate system where x_1 represents the tangential direction, x_2 is the thickness direction, and x_3 means the circumferential direction (Figure 3).

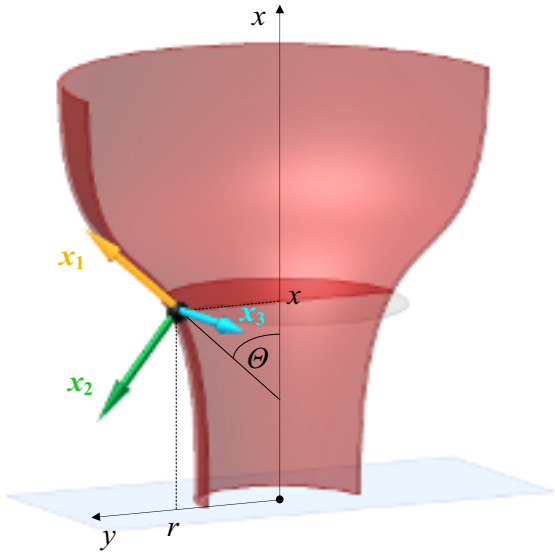

FIGURE 3. Cartesian coordinate system.

The mathematically, Pearson and Petrie formulation is given by the set of equations provided in Table 1.

TABLE 1. A full set of the Pearson and Petrie equations.

Equation type	Equation form	Equation number
Continuity equation	$\dot{m} = 2\pi r(x)h(x)v(x)\rho(T(x))$	(1)
Density	$\rho(T) = \dfrac{1}{\dfrac{R_g T}{P^* w} + b'}$	(2)
Internal bubble pressure	$\Delta P = \dfrac{h\sigma_{11}}{R_m} + \dfrac{h\sigma_{33}}{R_t}$	(3)
Curvature radius - tangential	$R_t = \dfrac{r}{\cos(\theta)}$	(4)
Curvature radius - circumferential	$R_m = \dfrac{-1}{\dfrac{d^2 r}{dx^2}\cos^3(\theta)}$	(5)

Equation type	Equation form	Equation number
Term	$\cos(\theta) = \frac{1}{\sqrt{1+\left(\frac{dr}{dx}\right)^2}}$	(6)
Force balance	$2\pi r h \sigma_{11} \cos(\theta) = F - \pi \Delta P \left(r_f{}^2 - r^2\right)$	(7)
Stress σ_{11}	$\sigma_{11}(x) = \frac{F - \pi \Delta P \left(r_f{}^2 - r(x)^2\right)}{2\pi r(x) h(x) \cos(\theta(x))}$	(8)
Tangential stress $\sigma_{11}(L)$ ***at the freeze line height***	$\sigma_{11}(L) = \frac{F}{2\pi R_1 H_1}$	(9)
Stress in the circumferential direction	$\sigma_{33}(x) = \frac{R_t(x)}{h(x)}\left(\Delta P - \frac{h(x)}{R_m(x)}\sigma_{11}(x)\right)$	(10)
Circumferential stress at the freeze line height	$\sigma_{33}(L) = \frac{R_1}{H_1}\Delta P$	(11)
Proportion between the total stresses, σ ***, and the extra stresses,*** τ	$\sigma_{11} = \tau_{11} - \tau_{22}$ $\sigma_{22} = 0$ $\sigma_{33} = \tau_{33} - \tau_{22}$	(12)

The meaning of the used symbols is following: x represents particular location at the bubble, $\dot{m}$ is the mass flow rate, $r(x)$ the bubble radius, $h(x)$ the film thickness, $v(x)$ the film velocity, $T(x)$ the temperature and $\rho(T)$ is the density (which is described below in more detail), ΔP is the internal bubble pressure, σ_{11} is the tangential directions of the stress, R_m is radius curvature, σ_{33} is circumferential directions of the stress, R_t is radius curvature , r_f is the bubble radius at the freeze line height, F means the take-up force, G stands for the gravity, and H is the force created by the air flow. The bubble radius at the freeze line height is, $R_1 = BURR_0$, and H_1 is the bubble thickness at the same place.

It should be mentioned that Eq. 2 for temperature dependent density has been derived by Spencer and Gilmore [33] with following symbol meaning: w *is* the molecular weight, R_g represents the universal gas constant (R_g = 8.314 J·K^{-1}·mol^{-1}), P^* is the cohesion pressure, and b' means the specific volume. As has been shown by Hellwege et al. [34], these parameters for PEs, takes the following forms: $w = 28 \cdot 10^{-3}$ *kg*·mol^{-1}, $b' = 8.75 \cdot 10^{-4}$ m^3·kg^{-1} and $P^* = 3.18 \cdot 10^8$ Pa. Putting all these numbers into the Eq. 2, the following equation for temperature dependent density raised:

$$\rho(T(x)) = \frac{10^3}{0.934 \cdot 10^{-3} T(x) + 0.875} \tag{13}$$

Main problem with the Pearson and Petrie formulation is the occurrence of numerical instabilities [24, 28, 31] and impossibility to represents real bubble shapes realistically [28, 31].

Numerical Instabilities

These types of instabilities are usually caused by inability of the numerical scheme to converge for certain polymer rheology, processing and boundary conditions or by existence of the multiple solutions. Moreover, the solution is very sensitive to the initial bubble angle at the die exit as well as to melt history which is related to the die flow. Due to that, the solution is available for only a small area of the operating conditions. This is discussed in more detail by Luo and Tanner [24].

Problems with the Bubble-Shape Description

These problems are connected with high stalk bubbles, i.e. bubbles with a long neck. Here, the bubble shape with the original elongated neck is not described exactly – the predicted values are set in earlier than the elongated neck of the bubble in reality [28, 31]. The presented problems of Pearson and Petrie formulation can be eliminated by the application of Zatloukal-Vlcek´s formulation derived through variational principles, which is described in the following parts in more detail.

Zatloukal-Vlcek Formulation

The Zatloukal and Vlcek formulation regards existence of the stable film blowing process as a situation which satisfies minimum energy requirements; otherwise, the bubble is viewed as unstable. The bubble is viewed as static flexible membrane having initially element length equal to dx (Figure 4), which is consequently deformed during the process by the internal load, p, and the take-up force, F (Figure 5).

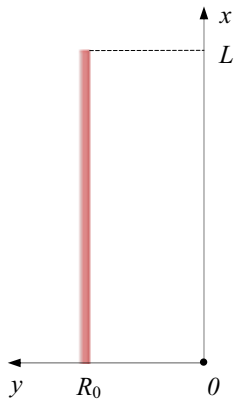

FIGURE 4. Membrane before deformation.

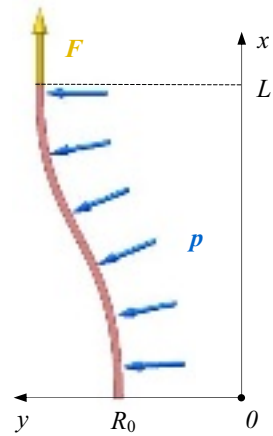

FIGURE 5. Membrane after deformation.

After the bubble deformation the element length is given by the following equation [28, 31]:

$$\sqrt{1+(y')^2}\,dx \approx \left[1+\frac{1}{2}(y')^2\right]dx \tag{14}$$

It has been shown in [28] that if the constant bubble compliance is assumed along the bubble, one can derive the analytical equation for the bubble shape satisfying the minimum-energy requirements by using variational principles. This model can be applied for description of different bubble types including high stalk bubbles [30]. In this work, bubble without neck will be considered only.

Bubble without Neck

The bubble without the neck is typical for LLDPE and LDPE polymers due to their higher melt strength [35]. Four parameters have to be known for the bubble shape description: freeze line height, L, bubble curvature, pJ (which is given by membrane compliance, J, and the internal load, p), the blow up ratio, BUR, and the die radius, R_0. In this case, Zatloukal-Vlcek model is given by the set of equations, which are provided in Table 2 and Table 3.

TABLE 2. A. Summary of the Zatloukal-Vlcek model for the bubble without neck.

Equation type	Equation form	Equation number
Differential equation	$Fy'' - \lambda_1 2\pi y + p = 0$	(15)
Bubble shape	$y = (R_0 - pJ)\cos\left(\frac{x\varphi}{L}\right) - \alpha'(pJ - BURR_0)\sin\left(\frac{x\varphi}{L}\right) + pJ$	(16)
Parameter	$x \in < 0; L >$	(17)
Parameter	$\alpha' = \sqrt{\frac{2pJ - R_0 - BURR_0}{pJ - BURR_0}\left\lvert\frac{R_0(BUR-1)}{pJ - BURR_0}\right\rvert}$	(18)
Parameter	$A = \frac{pJ - R_0}{pJ - BURR_0}$	(19)
Take-up force	$F = -\frac{L^2}{J\varphi^2}$	(20)
Internal bubble pressure	$\Delta p = \frac{pL}{2\pi\int_0^L y\sqrt{1+(y')^2}\,dx}$	(21)
Bubble compliance	$J = \frac{L^2 v_F}{2\eta\dot{\varepsilon}_1\varphi^2 Q}$	(22)

The symbol meaning is following: F is the take-up force, λ_1 stands for the Lagrange multiplier, p means the internal load. Parameter φ is given by a parameter (Eq. 19) according to Table 3.

TABLE 3. Parameters A and φ for different bubble shapes (y).

Equation	A	φ	y
1.	1	0	R_0
2.	$0 < A < 1$	$arctg\left(\frac{\sqrt{1-A^2}}{A}\right)$	The form of Eq. 16
3.	0	$\pi/2$	$R_0\left\{1-\sin\left(\frac{x\pi}{2L}\right)(1-BUR)\right\}$
4.	$-1 < A < 0$	$\pi + arctg\left(\frac{\sqrt{1-A^2}}{A}\right)$	The form of Eq. 16
5.	-1	π	$\frac{R_0}{2}\left\{1+\cos\left(\frac{x\pi}{L}\right)(1-BUR)+BUR\right\}$

Eqs. 9, 11, 16, 18-21 and Table 3 this work represents simple Zatloukal-Vlcek model for bubble without neck, which has to be combined with additional equations (energy equation, constitutive equation, Pearson and Petrie formulation for velocity calculation), which are described bellow in more detail.

Energy Equation

The assumption about the isothermal film blowing process is relaxed here by assuming the cross-sectionally average energy equation (the bubble is a quasicylinder at each point) taken from [36]:

$$\rho C_p \frac{dT}{dx} = -\frac{2\pi R\rho}{\dot{m}}\left[h\left(T-T_{air}\right)+\sigma_B\varepsilon\left(T^4-T_{air}^4\right)\right]+\tau:\nabla v+\rho\Delta H_f\frac{d\phi}{dx} \qquad (23)$$

where C_p stands for the specific heat capacity, ρ is the polymer density, R means the local bubble radius, h represents the heat transfer coefficient, T is the bubble temperature, T_{air} means the air temperature used for the bubble cooling , σ_B stands for the Stefan-Boltzmann constant, ε represents the emissivity, τ is the extra stress tensor, Δv means velocity gradient tensor, ΔH_f indicates the heat of crystallization per unit mass and ϕ is the average absolute degree of crystallinity of the system at the axial position, x.

In order to reduce the problem complexity, the axial conduction, dissipation, radiation effects and crystallization are neglected. For such simplifying assumptions, the Eq. 23 is reduced in the following, the simplest version of the cross-sectionally averaged energy equation:

$$\dot{m}C_p \frac{dT}{dx} = 2\pi y\left[h\left(T - T_{air}\right)\right] \tag{24}$$

where y is the bubble shape (given by Eq. 16 in Table 2), $\dot{m}$ represents the mass flow rate, h stands for the heat transfer coefficient, C_p is the specific heat capacity, T means the value of the bubble temperature and T_{air} represents the air temperature used for the bubble cooling. The Eq. 24 applied for the first part of the bubble takes the following form:

$$\int_{T_{die}}^{T_{solid}} \frac{\dot{m}C_p}{h\left(T - T_{air}\right)} dT = 2\pi \int_0^L y dx \tag{25}$$

where T_{die} and T_{solid} represents the temperature of the melt at the die exit and solidification temperature of the polymer, respectively. After integration from die temperature, T_{die}, up to freezeline temperature, T_{solid}, we can obtain equation defining the relationship between frezeline height, L, and heat transfer coefficient, h, which take the following simple analytical expression:

$$L = -\frac{1}{2}\dot{m}C_p \ln\left(-\frac{\left(T_{die} - T_{air}\right)}{\left(-T_{solid} + T_{air}\right)}\right)\frac{\varphi}{\pi h(\alpha pJ - \alpha BURR_0 - \sin(\varphi)R_0 - pJ\varphi + \sin(\varphi)pJ - \alpha\cos(\varphi)pJ + \alpha\cos(\varphi)BURR_0)} \tag{26}$$

With the aim to get equations for the temperature profile along the bubble, it is necessary to apply the Eq. 24 for any arbitrary point at the bubble i.e. in the following way:

$$\int_{T_{die}}^{T} \frac{\dot{m}C_p}{h\left(T - T_{air}\right)} dT = 2\pi \int_0^x y dx \tag{27}$$

After the integration of Eq. 27, the temperature profile takes the following analytical expression:

$$T = T_{air} + \left(T_{die} - T_{air}\right)\exp\left\{-\frac{2\pi Lh}{\dot{m}C_p\varphi}\left(-\alpha\left[R_0 BUR - pJ\right]\left[\cos\left(\frac{x\varphi}{L}\right) - 1\right] + \sin\left(\frac{x\varphi}{L}\right)\left[R_0 - pJ\right] + pJ\varphi\frac{x}{L}\right)\right\} \tag{28}$$

Constitutive Equations

Constitutive equations represent mathematical relationships which are derived from constitutive models containing various assumptions and idealizations about the molecular or structural forces and motions producing stress. Constitutive equations enable computing polymer melt stress response on the given flow field. Polymers, which lie between Newtonian liquids and Hookean solids, contain relatively long macromolecules and thus they cannot be described by simple physical laws [37-38].

In this work, the recently proposed generalized Newtonian model will be considered [38] with the aim to minimize the complexity of the film blowing problem. The main advantage behind this model is possibility to express all stress components as the analytical function of deformation rate even for complex flows where shear and extensional flows are mixed together. Moreover, specific form of the generalized Newtonian model, described below, allows taking both shear thinning as well as extensional viscosity strain hardening/thinning behavior properly into account [38]. The model takes the following form:

$$\tau = 2\eta D \tag{29}$$

where τ means the extra stress, D represents the deformation rate tensor and η stands for the viscosity, which is not constant (as in the case of standard Newtonian law), but it is allowed to vary with second, II_D, and third, III_D, invariants of deformation rate tensor according to Eq. 30

$$\eta\left(II_D, III_D\right) = \eta\left(II_D\right)^{f\left(III_D\right)} \tag{30}$$

where $\eta\left(II_D\right)$ and $f\left(T, III_D\right)$ are given by Eqs. 31 and 32

$$\eta\left(T, II_D\right) = \frac{\eta_0 a_T}{\left[1 + \left(\lambda a_T II_D\right)^a\right]^{\left(\frac{1-n}{a}\right)}} \tag{31}$$

$$f\left(T, III_D\right) = \left[\frac{tanh\left(\alpha a_t \sqrt[3]{4\left|III_D\right|} + \beta\right)}{tanh(\beta)}\right]^{\xi} \tag{32}$$

where η_0, λ, a, n, β, α and ξ are adjustable parameters. Note that α is so called extensional strain hardening parameter. The uniaxial extensional viscosity, needed for model parameters identification process, is given by the following form:

$$\eta_E = \frac{\tau_{xx} - \tau_{yy}}{\dot{\varepsilon}} \tag{33}$$

where $\dot{\varepsilon}$ is extensional strain rate.

It should be mentioned that the temperature effect on the polymer melt rheology is taken into account through shift factor, a_T, defined through the following well known Arrhenius equation:

$$a_T = exp\left[\frac{E_a}{R}\left(\frac{1}{273.15+\bar{T}} - \frac{1}{273.15+T_r}\right)\right] \tag{34}$$

where E_a is the activation energy, R is the universal gas constant, T_r is the reference temperature and T is temperature given by the Eq. 28.

Velocity Profile

With the aim to calculate the velocity profile and the film thickness in the non-isothermal film blowing process, the force balance in vertical direction (gravity and upward force due to the airflow are neglected) proposed by Pearson and Petrie is considered in the following form:

$$\frac{2\pi y h \sigma_{11}}{\sqrt{1+(y')^2}} = F - \pi \Delta p \left(R_0^2 BUR^2 - y^2 \right) \tag{35}$$

where σ_{11} is the total stress in the machine direction and F and Δp are defined by Eqs. 20 and 21 in Table 2. The deformation rate tensor in the bubble forming region takes the following form:

$$D = \begin{pmatrix} \dot{\varepsilon}_1 & 0 & 0 \\ 0 & \dot{\varepsilon}_2 & 0 \\ 0 & 0 & \dot{\varepsilon}_3 \end{pmatrix} \tag{36}$$

where the following deformation rate approximations have been used:

$$\dot{\varepsilon}_1 = \frac{dv_x}{dx} \approx \overline{\dot{\varepsilon}_1} = \frac{1}{L}\int_0^L \dot{\varepsilon}_1 dx \tag{37}$$

$$\dot{\varepsilon}_2 = \frac{v}{h}\frac{dh}{dx} \approx \overline{\dot{\varepsilon}_2} = \frac{\overline{v}}{\overline{h}}\frac{\overline{h} - H_0}{L} \tag{38}$$

$$\dot{\varepsilon}_3 = -\left(\dot{\varepsilon}_1 + \dot{\varepsilon}_2\right) \approx \overline{\dot{\varepsilon}_3} = -\left(\overline{\dot{\varepsilon}_1} + \overline{\dot{\varepsilon}_2}\right) \tag{39}$$

where v is velocity, v_f represents bubble velocity at the freezeline height, v_d is bubble velocity at the die, L is freezeline height, H_0 is bubble thickness at the die. Here, $\overline{v}$ and $\overline{h}$ is velocity mean value along the bubble and thickness mean value along the bubble, respectively, which are defines as follows:

$$\overline{v} = \frac{1}{L}\int_0^L v(x)dx \tag{40}$$

$$\overline{h} = \frac{1}{L}\int_0^L h(x)dx \tag{41}$$

Assuming that $h << y$, then

$$\sigma_{11} = \tau_{11} - \tau_{22} \tag{42}$$

By combination of Eqs. 23, 34, 42, the σ_{11} takes the following form:

$$\sigma_{11} = 2\eta\left(2\frac{dv}{dx} + \frac{v}{y}y' \right) \tag{43}$$

After substituting Eq. 43 into Eq. 34, the equation for the bubble velocity in the following form can be obtained.

$$v = v_{die}\, exp\left(\int_0^L \left\{ \frac{\sqrt{1+(y')^2}\left[F - \pi\Delta p\left(R_0^2 BUR^2 - y^2\right)\right]}{4Q\eta a_T} - \frac{1}{2y}y' \right\} dx \right) \tag{44}$$

Having the velocity profile, the deformation rates and the thickness can be properly calculated along the bubble.

Numerical Scheme

First, model is focused on the non-isothermal film blowing process. Non-isothermal conditions are expressed with the help of the Eq. 28, where the temperature profile is calculated for the constant heat transfer coefficient, *h*, stated inside the Eq. 26 for the constant freeze line height, *L*. Second, the polymer material is assumed as a non-Newtonian material. Viscosity is expressed by the representative 'bubble viscosity - $\overline{\eta}$' considering average bubble temperature, $(T_{die}+T_{solid})/2$, with corresponding average Arrhenius temperature shift factor, $a_{TSj,}$ and components of the deformation rate tensor through second and third invariant of deformation rate tensor (see Eqs. 45 and 46).

$$II_D = \sqrt{2\left(\dot{\varepsilon}_1^2 + \dot{\varepsilon}_2^2 + \dot{\varepsilon}_3^2\right)} \tag{45}$$

$$III_D = |\dot{\varepsilon}_1 \dot{\varepsilon}_2 \dot{\varepsilon}_3| \tag{46}$$

Third, the velocity profile was proposed as a non-linear profile between the die and the freeze line height. Although, this is described in the previous section, to take the temperature profile correctly into account during velocity calculation, representative bubble viscosity is multiplied by the Arrhenius temperature shift factor, a_T, in the Eq. 44. Last, the calculation is given only for bubble without neck.

Two numerical schemes have been tested. In the first one, bubble shape, *pJ*, has been fixed and Δp, *F* were unknown parameters whereas in the second one internal bubble pressure, Δp, was fixed and bubble shape, *pJ,* and take-up force, *F*, were taken as unknown variables.

In the case of a constant bubble shape, *pJ*, the calculation started by the initial proposal of viscosity for a linear velocity and thickness profile along the bubble. With this value of viscosity divided by a mean value of Arrhenius temperature shift factor (Eq. 47), a_{TS}, the non-linear velocity, thickness and temperature profiles are counted for the drawn force, which satisfy the condition of equality between a velocity at the freeze line height, $v_{F,}$ and calculated velocity for non-linear profile, *v*.

$$a_{TS} = \frac{1}{L}\int_0^L a_T\, dx \tag{47}$$

As soon as the condition is reached, a new value of viscosity is obtained with the second and third invariants. In the case, where the viscosity is not stable and equal to

the previous value, the computational process is repeated to find out a new take-up force, otherwise, a new internal bubble pressure is adjusted. If the previous and new internal bubble pressures are not equal, the completely whole computational process is repeated. In an opposite case, the final bubble shape, velocity and temperature profiles are created.

In the second numerical scheme, the procedure is almost the same, only with difference, that internal bubble pressure, Δp, is fixed and bubble shape, pJ, and take-up force, F, are taken as unknown variables. It has been found that both numerical schemes yield almost the same results and thus the second numerical scheme has been utilized in this work.

RESULTS AND DISCUSSION

At the beginning of the research, it is necessary to check, whether Zatloukal-Vlcek non-isothermal model for non-Newtonian polymer melts has capability to describe experimental reality with respect to bubble shape, velocity and temperature profiles. For the film blowing model test, experimental data for LDPE (material L8 – experiment 29) provided in the Tas's Ph.D. thesis [16] were used. As the first step, the rheological characteristics of the LDPE material taken from [16] were fitted by the generalized Newtonian model (Eq. 30).

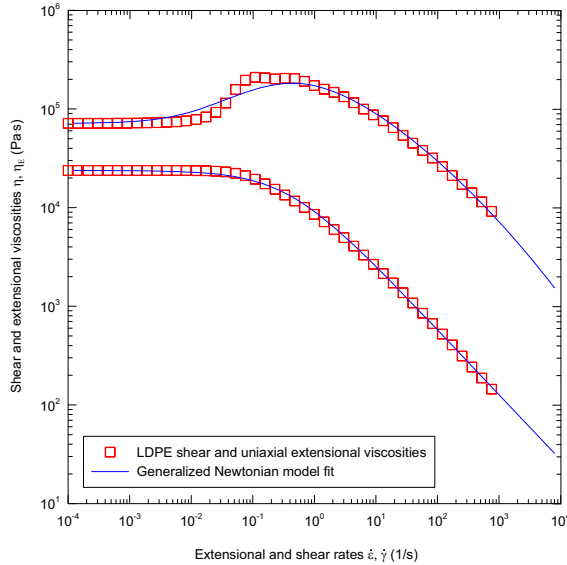

FIGURE 6. Comparison between generalized Newtonian model fitting lines and experimental data for LDPE material taken from Tas's Ph.D. thesis [16].

Figure 6 clearly shows that the used generalized Newtonian model can describe extensional as well as shear viscosity data very well. All model, LDPE material and processing parameters for chosen processing conditions are summarized in Tables 4-6.

TABLE 4. Zatloukal-Vlcek film blowing model parameters used in the model testing on the Tas's Ph.D. thesis data for LDPE L8 for exp. 29 [16].

BUR (-)	L (m)	Δp (Pa)	R_0 (m)	H_0 (m)	TUR (-)	$\dot{m}$ ($kg \cdot h^{-1}$)
2.749	0.138816	70	0.0178	0.0022	19.444	0.001

TABLE 5. Parameters of the generalized Newtonian constitutive equation.

η_0 (Pa.s)	a (-)	n (-)	α (s)	β (-)	λ (s)	ξ (-)
2365	0.71597	0.37108	0.00001	$9.70 \cdot 10^{-7}$	0.17242	0.041915

TABLE 6. Temperature parameters.

T_{air} (°C)	T_{solid} (°C)	T_{die} (°C)	T_r (°C)	E_a ($J.mol^{-1}$)	R ($J \cdot K^{-1} \cdot mol^{-1}$)	C_p ($J.kg^{-1}.K^{-1}$)
25	92	145	190	59000	8.314	2300

For the above presented parameters, the Figures 7-9 were generated. In more detail, the Zatloukal-Vlcek model predictions for the bubble shape (Figure 7), velocity (Figure 8) and temperature profiles (Figure 9) are compared with Tas's experimental data [16] together with theoretical predictions by Beaulne and Mitsoulis model [13] and Sarafrazi and Sharif [14] model. Based on the Figures 7-9 and Table 7, it is nicely visible that the predictions of the Zatloukal-Vlcek model are in very good agreement with the experimental data.

a)

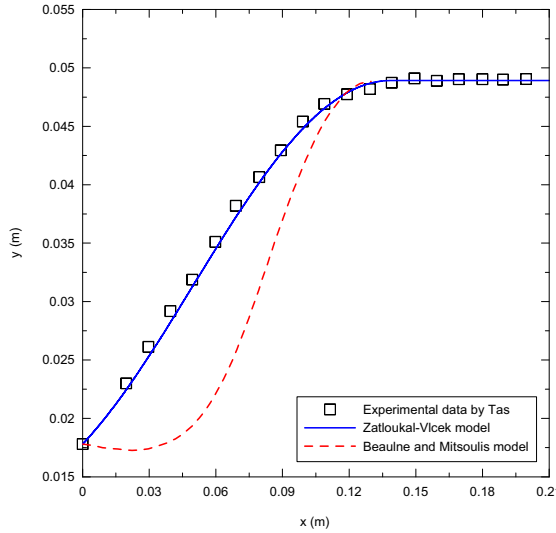

b)

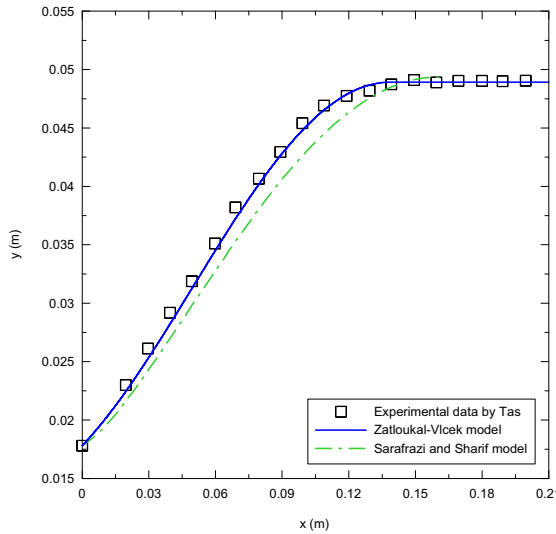

FIGURE 7. Comparison of the bubble shape between the Zatloukal-Vlcek model prediction [28], experimental data for the LDPE L8 taken from Tas´s Ph.D. thesis [16] and (a) the Beaulne and Mitsoulis model prediction [13]; (b) the Sarafrazi and Sharif model prediction [14].

a)

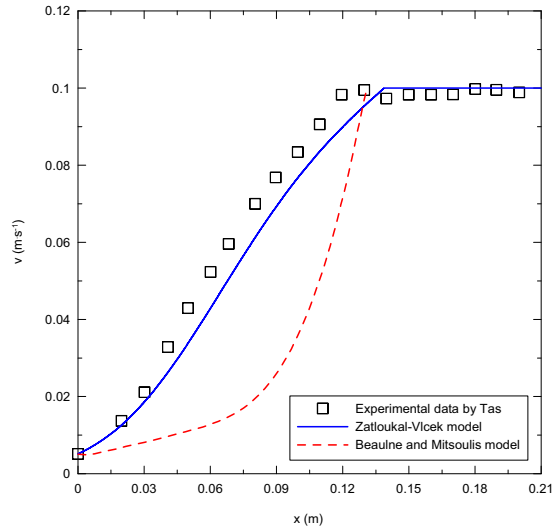

b)

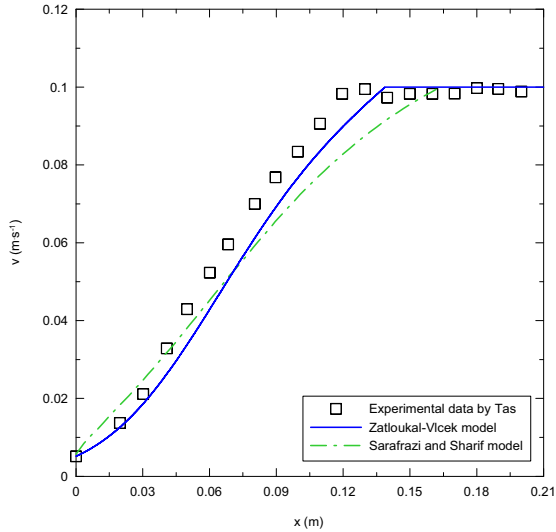

FIGURE 8. Comparison of the bubble velocity-profile between the Zatloukal-Vlcek model prediction [28], experimental data for the LDPE L8 taken from Tas´s Ph.D. thesis [16] and (a) the Beaulne and Mitsoulis model prediction [13]; (b) the Sarafrazi and Sharif model prediction [14].

a)

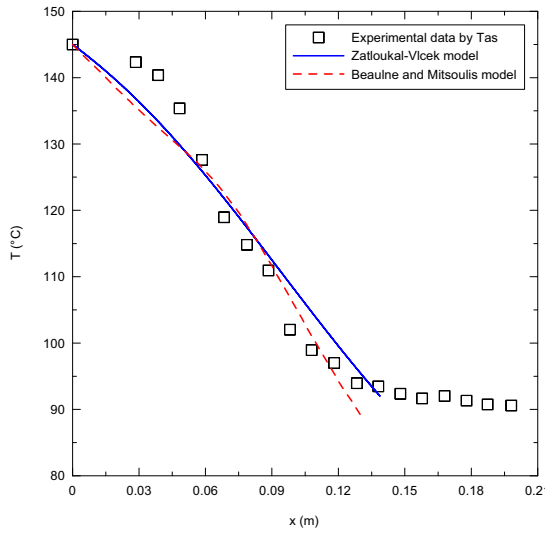

b)

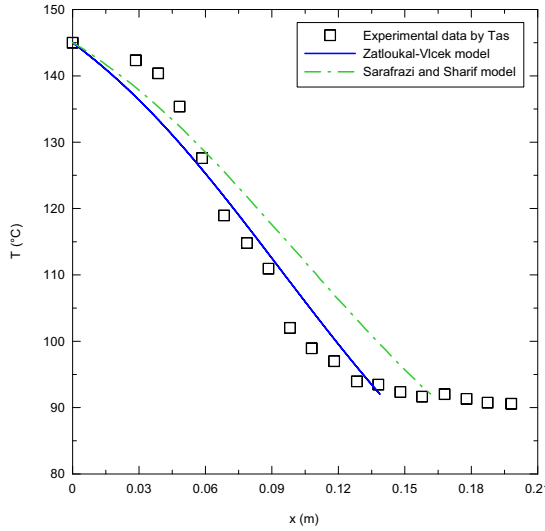

FIGURE 9. Comparison of the bubble temperature-profile between the Zatloukal-Vlcek model prediction [28], experimental data for the LDPE L8 taken from Tas´s Ph.D. thesis [16] and (a) the Beaulne and Mitsoulis model prediction [13]; (b) the Sarafrazi and Sharif model prediction [14].

It is nicely visible that Zatloukal-Vlcek model bubble shape, velocity, temperature and lock in stresses at the freeze line σ_{11}, σ_{33} predictions (see Figures 7-9 and Table 7) are in good agreement with experimental.

TABLE 7. Comparison between experimental data by Tas [16] and prediction data by the Zatloukal-Vlcek model [28] and two comparing models.

Models	Δp (Pa)	F (N)	σ_{11} (MPa)	σ_{33} (MPa)
Experimental data (Tas)	70.00	3.50	2.70	0.700
Zatloukal-Vlcek	70.00	6.89	5.44	0.830
Sarafrazi and Sharif	55.84	3.34	3.11	0.375
Beaulne and Mitsoulis	168.00	2.13	2.06*	2.446*

* The values are calculated by our self according to the parameters provided in Beaulne and Mitsoulis work [13].

Complete set of calculated variables in Zatloukal-Vlcek model for the theoretical predictions depicted in Figures 7-9 is summarized in Table 8. Just note that for the die volume rate calculation (from the experimentally known mass flow rate), the following definition of the LDPE density was used

$$\rho = \frac{1000}{0.934 \cdot 0.001 \cdot (273.15 + T_{DIE}) + 0.875} \tag{48}$$

TABLE 8. Complete set of calculated variables in Zatloukal-Vlcek model.

F (N)	pJ (m)	v_D ($m \cdot s^{-1}$)	v_F ($m \cdot s^{-1}$)	J (Pa^{-1})	h ($W \cdot m^{-2} \cdot K^{-1}$)	η ($Pa \cdot s$)	η_s ($Pa \cdot s$)	a_{TS} (-)	a_{TSj} (-)
6.89	0.0298178	0.0051	0.1	0.00198	42.752	4414.5	89758.9	20.33	16.39

CONCLUSION

In this work, film blowing process analysis has been performed theoretically by using minimum energy approach for non-Newtonian polymer melts considering non-isothermal processing conditions and the obtained predictions were compared with both, theoretical and experimental data (bubble shape, velocity and temperature profiles) taken from the open literature.It has been found that model predictions are in very good agreement with the corresponding experimental data.

ACKNOWLEDGMENTS

The authors wish to acknowledge GA CR and the Ministry of Education CR for the financial support of Grant No. 103/09/2066 and MSM 7088352101, respectively.

REFERENCES

1. S. Kim, Y.L. Fang, P. G. Lafleur and P. J. Carreau, *Polym. Eng. Sci.* **44**, 283 (2004).
2. C. D. Han and J. Y. Park, *J. Appl. Polym. Sci.* **19**, 3277 (1975).
3. C. D. Han and J. Y. Park, *J. Appl. Polymer Sci.* **19**, 3291 (1975).
4. Y. L. Yeow, *J. Fluid Mech* **75**, 577 (1976).
5. C. D. Han and R. Shetty, *Ind. Eng. Chem. Fund.* **16,** 49 (1977).
6. T. Kanai and J. L. White, *Polym. Eng. Sci.* **24**, 1185 (1984).
7. W. Minoshima and J. L. White, *J. Non-Newtonian Fluid Mech.* **19**, 275 (1986).
8. T. Kanai and J. L. White, *J. Non-Newtonian Fluid Mech.* **19**, 275 (1986).
9. T. J. Obijeski and K. R. Puritt, *SPE ANTEC Tech. Papers* 150 (1992).
10. P. A. Sweeney and G. A. Campbell, *SPE ANTEC Tech. Papers* 461 (1993).
11. T. Kanai and G. A. Campbell, *Film Processing: Progress in Polymer Processing*, Munich: Hanser Gardner Publications, 1999.
12. T. I. Butler, *SPE ANTEC Tech. Papers* 1120 (2000).
13. M. Beaulne and E. Mitsoulis, *J. Appl. Polym. Sci.* **105**, 2098-2112 (2007).
14. S. Sarafrazi and F. Sharif, *International Polymer Processing.* **23**, 30-37 (2008).
15. I. A. Muslet and M. R. Kamal, *J. Rheol.* **48**, 525-550 (2004).
16. P. P. Tas, "Film blowing from polymer to product", Ph.D. Thesis, Technische Universitat Eindhoven, 1994.
17. R. K. Gupta, "A new non-isothermal rheological constitutive equation and its application to industrial film blowing", Ph.D. Thesis, University of Delaware, 1981.
18. J. R. A. Pearson and C.J.S. Petrie, *J. Fluid. Mech.* **40**, 1 (1970).
19. J. R. A. Pearson and C.J.S. Petrie, *J. Fluid. Mech.* **42**, 609 (1970).
20. J. R. A. Pearson and C.J.S. Petrie, *Plast. Polym.* **38**, 85 (1970).
21. C. J. S. Petrie, "Film blowing, blow moulding and thermoforming," in *Applied Science*, edited by J. R. A. Pearson and S.M. Richardson, London, 1983, p. 217.
22. C. D. Han and J. Y. Park, *J. Appl. Polym. Sci.* **19**, 3277 (1975).
23. C. J. S. Petrie, *Am. Inst. Chem. Eng. J.* **21**, 275 (1975).
24. X. L. Luo and R. I. Tanner, *Polym. Eng. Sci.* **25**, 620 (1985).
25. B. K. Ashok and G. A. Campbell, *Int. Polym. Proc.* **7**, 240 (1992).
26. S. M. Alaie and T. C. Papanastasiou, *Int. Polym. Proc.* **8**, 51 (1993).
27. J. M. Andr´e, Y. Demay, J. M. Haudin, B. Monasse and J. F. Agassant, *Int. J. Form. Proc.* **1**, 187 (1998).
28. M. Zatloukal and J. Vlcek, *J. Non-Newtonian Fluid Mech.* **123**, 201-213 (2004).
29. M. Zatloukal, H. Mavridis, J. Vlcek and P. Saha, *SPE ANTEC*, Charlotte, USA, 2006, p. 825-829.
30. M. Zatloukal and J. Vlcek, *J. Non-Newtonian Fluid Mech.* **133**, 63-72 (2006).
31. M. Zatloukal, P. Saha, Modeling of the film blowing process by using variational principles for high stalk bubbles. PPS-21, Leipzig, Germany, 2005 (CD-ROM).
32. R. S. Mayavaram, "Modeling and simulation of film blowing process", Ph.D. Thesis, A&M University Texas, 2005.
33. R. S. Spencer and R.D. Gilmore, *J. Appl. Phys.* 21-523 (1950).
34. K. H. Hellwege, W. Knappe, P. Lehmann and Z. Kolloid, *Polymere* **183**, 110-120 (1962).
35. K. Cantor, *Blown Film Extrusion*, Munich: Cark Hanser Verlag, 2006, p. 165.
36. A. K Doufas and A.J. McHugh, *J. Rheol.* **45**, 1085 (2001).
37. M. Zatloukal, *J. Non-Newtonian Fluid Mech.* **113**, 209 (2003).
38. M. Zatloukal, H. Mavridis, J. Vlcek and P. Saha, *SPE ANTEC*, 1579-1583 (2007).